Mon. Not. R. Astron. Soc. **385,** 728–736 (2008) doi:10.1111/j.1365-2966.2008.12894.x

Cosmic reionization in dynamic quintessence cosmology

D. Crociani,[1⋆] M. Viel,[2,3] L. Moscardini,[1,4] M. Bartelmann[5] and M. Meneghetti[6]

[1]*Dipartimento di Astronomia, Università di Bologna, via Ranzani 1, I-40127 Bologna, Italy*
[2]*INAF – Osservatorio Astronomico di Trieste, via G.B. Tiepolo 11, I-34131 Trieste, Italy*
[3]*INFN/National Institute for Nuclear Physics, Sezione di Trieste, via Valerio 2, I-34127 Trieste, Italy*
[4]*INFN/National Institute for Nuclear Physics, Sezione di Bologna, viale Berti Pichat 6/2, I-40127 Bologna, Italy*
[5]*Zentrum für Astronomie, ITA, Universität Heidelberg, Albert-Überle-Str. 2, D-69120 Heidelberg, Germany*
[6]*INAF – Osservatorio Astronomico di Bologna, via Ranzani 1, I-40127 Bologna, Italy*

Accepted 2007 December 20. Received 2007 December 18; in original form 2007 August 30

ABSTRACT

In this paper, we investigate the effects that a dynamic dark energy component dominant in the universe at late epochs has on reionization. We follow the evolution of H II regions with the analytic approach of Furlanetto & Oh in two different universes for which we assume the Peebles & Ratra and Brax & Martin quintessence models and we compare our results to the Λ cold dark matter (ΛCDM) scenario. We show that, for a fixed ionization efficiency, at the same cosmological epoch the morphology of bubbles is dominated by high-mass objects and the characteristic size of the ionized regions is slightly smaller than in the ΛCDM model, especially at the latest stages of reionization, due to the higher recombination efficiency. As a consequence, the bubbles' 'epoch of overlap' happens earlier than in ΛCDM. Finally, we show how the different evolution of the H II regions affects the transmission of the high-z quasi-stellar object spectra, reducing the Lyman flux absorption at small optical depths.

Key words: galaxies: evolution – intergalactic medium – cosmology: theory.

1 INTRODUCTION

Reionization of the intergalactic medium (IGM) is a crucial epoch for the history of the universe, when the neutral gas produced at recombination is ionized by the ultraviolet (UV) radiation emitted by the first luminous sources. After this stage, the IGM contains a small amount of neutral gas, responsible for the absorptions in the spectra of background objects. Reionization is still a poorly understood process because of the unknown nature of the ionizing sources and of the complex physical mechanisms producing the radiation emission. However, as suggested by recent observations, it turns out to be better described as a spatially inhomogeneous and not instantaneous phase (see e.g. Ciardi & Ferrara 2005, and references therein).

While the Lyman α transmitted flux in the high-z quasar [quasi-stellar object (QSO)] spectra found by the Sloan Digital Sky Survey suggests that the end of reionization is at $z \sim 6$ (Becker et al. 2001; Fan et al. 2001; White et al. 2003; Fan et al. 2006), the last results from the cosmic microwave background (CMB) polarization provide a Thompson optical depth of $\tau = 0.09 \pm 0.03$ that requires the completion of the reionization process at $z \sim 10$ (Spergel et al. 2007). On the other hand, the IGM temperature measurements at $z < 4$ (Hui & Haiman 2003) show that the reionization epoch occurs at $6 < z < 10$, while the lack of evolution in the Lyman α galaxy luminosity function at $5.7 \lesssim z \lesssim 6.5$ suggests that probably half of the IGM is ionized at $z \sim 6.5$ (Malhotra & Rhoads 2004). More recent estimates, based on high-z HIRES QSOs, seem instead to argue against sudden changes in the IGM properties due to late reionization at $z \sim 6$ (Becker, Rauch & Sargent 2007): it is worth stressing, however, that the use of QSO near zones to probe the IGM ionization fraction could still be problematic (see e.g. Bolton & Haehnelt 2007).

Future observations, such as Lyman α galaxy surveys (Kashikawa et al. 2006), measurements of the CMB polarization and of the Sunyaev–Zeldovich effect that will be obtained by the *Planck* satellite and, more importantly, neutral hydrogen 21-cm observations through new generation telescopes (LOFAR, SKA), must provide further information to constrain the reionization scenario. In recent years, several analytic, semi-analytic and numerical models (see e.g. Gnedin 2000; Ciardi, Ferrara & White 2003; Haiman & Holder 2003; Wyithe & Loeb 2003; Barkana & Loeb 2004; Madau et al. 2004; Choudhury & Ferrara 2006; Iliev et al. 2007; Wyithe & Cen 2007) have been developed in order to describe how the first sources of UV radiation impact on the IGM. The basic assumption of these approaches is to model the relations between the H II regions, the ionizing sources that allow to describe the morphology of bubbles, and the galactic physics, such as gas cooling, star formation, radiative feedback and radiative transfer. Despite some controversial results, the reionization process fits reasonably well in a 'standard' Λ cold

⋆E-mail: daniela.crociani2@studio.unibo.it

dark matter (ΛCDM) cosmology, that is, in a model where CDM and baryon density fluctuations grow in a flat universe dominated at late epochs by a dark energy component, consisting in cosmological constant. The latter is characterized by a constant equation of state $p = w\rho c^2$, with $w = -1$.

At present, the best probe of dark energy is provided by Type Ia supernovae (SNeIa). However, even including the most recent high-z observations (see e.g. Riess et al. 2007), it is still not possible to obtain a high-precision determination of the dark energy equation. Tight constraints could only be put if strong and unjustified priors on its evolution are assumed. While observations suggest that $w \sim -1$ at late epochs, the time-evolution of the dark energy component is basically not constrained. The so-called quintessence models, where w is varying in time, are not excluded. In the CDM cosmologies with dynamic dark energy, the main consequence of having $w > -1$ at high z is the earlier growth of the matter fluctuations. This determines a higher number density of haloes in the quintessence universe than in the standard cosmology at a fixed epoch (see e.g. Maio et al. 2006). Thereby, the presence of a dark energy component might affect the reionization process, requiring a different ionization efficiency to fully ionize the IGM at a given redshift.

In this work, we use an analytic approach to investigate how reionization proceeds in quintessence cosmologies. In doing this, we consider two different cosmological models for which we assume that the redshift dependence of the equation of state parameter $w(z)$ follows the self-interacting potentials proposed by Peebles & Ratra (2003) and Brax & Martin (2000). The predicted scenario obtained by 'painting' the evolution of the H II regions through the (Furlanetto & Oh 2005, hereafter F05) analytic model is compared to that expected for a ΛCDM universe.

This paper is organized as follows. In Section 2, we briefly outline the quintessence cosmologies considered here. In Section 3, we review the main features of the F05 model. Section 4 contains the results on the evolution of the ionized bubbles and their properties. The final Section 5 summarizes our main conclusions.

2 PROBING THE DYNAMIC QUINTESSENCE COSMOLOGY

The main aim of this paper is to investigate the process of cosmic reionization in quintessence cosmologies and compare to the predicted scenario for a standard flat ΛCDM universe. Thus, the ΛCDM cosmology will be our reference case, for which we assume that the contributions to the present density parameter from cosmological constant, matter and baryons are $\Omega_{0\Lambda} = 0.7, \Omega_{0\rm m} = 0.3$ and $\Omega_{0\rm b} = 0.046$, respectively; the Hubble constant is $H_0 = 70\,{\rm km\,s^{-1}\,Mpc^{-1}}$ (i.e. $h = 0.7$ in units of $100\,{\rm km\,s^{-1}\,Mpc^{-1}}$). We also fix the normalization of the power spectrum of the matter fluctuations according to $\sigma_8 = 0.9$ and the spectral index is $n = 1$. These parameters are in agreement with the *WMAP* first-year data (Spergel et al. 2003). We recall that the more recent analysis of the *WMAP* three-year data (Spergel et al. 2007) suggests slightly different values (in particular a lower σ_8 and a smaller $\Omega_{0\rm m}$). Our parameter choice, which is done to allow a direct comparison with the similar analysis made by F05, can have some small quantitative effect on some of the results, but cannot alter the general conclusions of our analysis, which is aimed at discussing the expected differences between models where the dark energy component is provided by a cosmological constant or by a dynamic quintessence.

Thus, the dark energy models we consider are cosmological scenarios in which the dynamic dark energy component is characterized by a self-interacting scalar field Φ, evolving under the effects of the potential $V(\Phi)$. Here, we summarize the main features of these models (see Peebles & Ratra 2003, for more details).

The potential has to satisfy the Klein–Gordon equation

$$\ddot{\Phi} + 3H(z)\dot{\Phi} + \frac{\partial V}{\partial \Phi} = 0, \tag{1}$$

where $H(z)$ represents the redshift evolution of the Hubble constant given by the usual Friedmann equation.

The corresponding z-evolution of the quintessence parameter w is provided by the equation of state

$$w \equiv \frac{p}{\rho c^2} = \frac{\frac{\dot{\Phi}^2}{2} - V(\Phi)}{\frac{\dot{\Phi}^2}{2} + V(\Phi)}, \tag{2}$$

such that $w \to -1$ if $\dot{\Phi}^2 \ll V(\Phi)$. Many analytic expressions have been proposed for the potential $V(\Phi)$. They describe the present dark energy amount simply by setting their amplitude on the initial conditions and determine different redshift evolutions for w. In our analysis, we use the potentials proposed by Peebles & Ratra (2003) (hereafter RP):

$$V(\Phi) = \frac{k}{\Phi^\alpha}, \tag{3}$$

and by Brax & Martin (2000):

$$V(\Phi) = k\Phi^{-\alpha} \exp\left(\frac{\Phi^2}{2}\right), \tag{4}$$

as suggested by supergravity theory (hereafter SUGRA); k has dimension of mass raised to the power $(\alpha + 4)$. The values for k and α are fixed by assuming a flat universe with a dark energy contribution to the present density parameter $\Omega_{0\rm de} = 0.7$, and $w_0 \equiv w(z = 0) = -0.85$ and -0.83 for SUGRA and RP potentials, respectively. These choices for w_0, even if only marginally consistent with the observational constraints (see e.g. Riess et al. 2007), have been made with the purpose of emphasizing differences with the ΛCDM model. The remaining parameters have been fixed to those of the ΛCDM model: $h = 0.7, \sigma_8 = 0.9$ and $n = 1$. Note that the quintessence models here considered do not violate the constraints recently obtained from the *WMAP* three-year data (Spergel et al. 2007) for the electron scattering optical depth

$$\tau_{\rm e} = \int_0^{z_{\rm r}} n_{\rm e}(z)\sigma_{\rm T}\frac{{\rm d}L(z)}{{\rm d}z}{\rm d}z, \tag{5}$$

computed at the reionization epoch, assumed to be $z_{\rm r} = 6$. In the previous equation, $\sigma_{\rm T}$ represents the Thompson scattering cross-section, and $n_{\rm e}(z)$ and $L(z)$ are the electron density and the comoving distance, respectively. In more detail, we estimate for the ΛCDM, RP and SUGRA models $\tau_{\rm e} = 0.132, 0.130$ and 0.125, which agree (at 1.5σ level) with the *WMAP* optical depth. Among all the possible dark energy models, we concentrate on these two since they have been accurately investigated by other authors under the theoretical point of view and their impact on observational quantities have been extensively addressed (see e.g. Dolag et al. 2004; Meneghetti et al. 2005). Furthermore, deviations from the ΛCDM behaviour are larger at high redshifts, in an interesting regime for the reionization analysis made here. This is evident by looking at the time-evolution of the equation-of-state parameter w, shown in the upper panel of Fig. 1. Though the RP and SUGRA display similar values for w today, strong differences appear at high redshifts. Parametrizing the evolution of w in terms of the expansion factor a as $w(a) = w_0 + w_a(1 - a)$, we find that the RP and SUGRA models can be fitted by $w_a \sim 0.08$ and 0.55, respectively. These values are still consistent with the present observational constraints. For example, Liddle

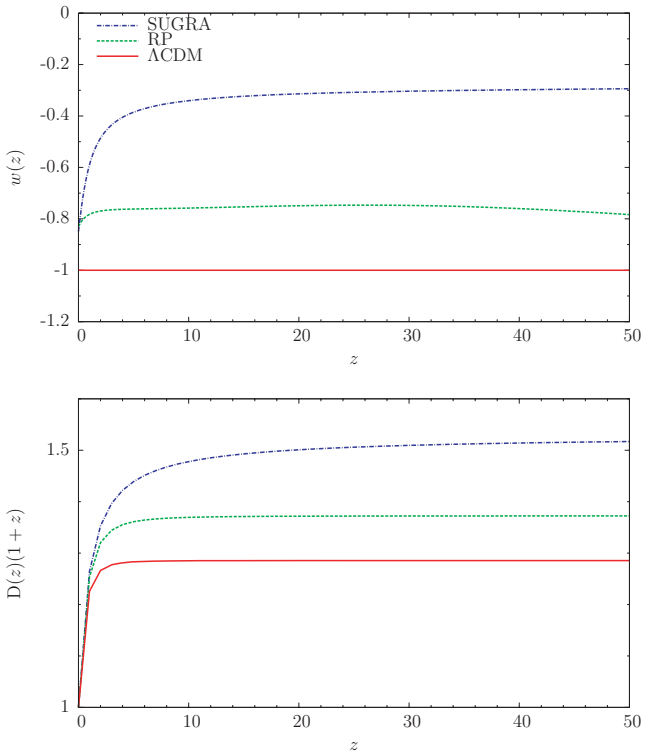

Figure 1. Redshift evolution of the cosmic equation-of-state parameter w (top panel) and of the growth factor, given in terms of $D(z)(1 + z)$ and normalized to its value at the present time (bottom panel). Different lines refer to ΛCDM model (solid line), RP model (dashed line) and SUGRA model (dot–dashed line).

et al. (2006) combining data from CMB, SNIa and baryonic acoustic oscillations found $w_a = 0.0 \pm 0.8$. Of course, our results will depend on the considered dark energy scenarios: models having parameters more similar to (different from) the ΛCDM cosmology (for which $w_0 = -1, w_a = 0$) would show smaller (larger) effects on the observables discussed here. These high-redshift differences affect the initial phases of the reionization process. In particular,we expect that at the redshifts of interest ($z \gtrsim 6$) the RP model behaves as an 'intermediate case' between SUGRA and ΛCDM. Note that in quintessence cosmologies, the growth factor $D(z)$ is larger than in the standard cosmology, as shown in the lower panel of Fig. 1, where the quantity $D(z)(1 + z)$ has been normalized to its value at the present time. Thus, the main effects of having $w > -1$ at high redshifts are an earlier formation of the structures and a higher abundance of haloes than in the ΛCDM cosmology at a fixed epoch (see the discussion in Maio et al. 2006). As an illustrative example, in Fig. 2 we show the distribution of the dark matter halo sizes as predicted by the Press & Schechter (1974) (hereafter PS74) theory for the ΛCDM (solid line), RP (dashed line) and SUGRA (dot–dashed line) cosmologies at three different redshifts. Indeed, at the same cosmological epoch, the halo distribution is dominated by larger objects in the quintessence cases, in particular in the SUGRA model. This can strongly affect the ionization process of the universe. Indeed numerical simulations (Ciardi et al. 2003; Sokasian et al. 2003, 2004) showed that reionization is an 'inside–out' phenomenon, that is, it begins in overdense regions and expands in underdense regions: this property predominantly originates from the fast increase in the abundance of ionizing sources. However, we remark that a slower (or vanishing) change in the source population should cause a rapid escape of the ionizing photons towards the external underdense regions: in this case reionization would be an outside–in process.

3 AN ANALYTIC APPROACH TO COSMIC REIONIZATION

To investigate how reionization occurs, we use the analytic approach proposed by F05. In this section, we review the main features of the model: for further details we refer to the original paper and to Furlanetto et al. (2004a) (hereafter F04).

3.1 Evolution of bubbles without recombination

The evolution of the ionized bubbles is determined by the hierarchic growth of matter fluctuations. This can be described by making use of the extended PS74 formalism (Lacey & Cole 1993). A warning has to be kept in mind about the use of the Press & Schechter mass function that is proven to not work well for rare haloes at high redshifts. In particular, numerical simulations (see e.g. Iliev et al. 2006; Lukic et al. 2007; Reed et al. 2007) show that it underestimates their abundance by a significant factor, with not negligible effects on the bubble distribution. However, we recall that the extended formalism has not been developed for mass functions different from PS74: for this reason we have to rely on it, even if this can affect some of the the following results.

In the PS74 scenario, at a fixed cosmological epoch, an ionized bubble grows around a galaxy of mass $m_{\rm gal} \geqslant m_{\rm min}(z)$, where $m_{\rm min}(z)$ represents the virial mass corresponding to $T = 10^4$K, the temperature at which hydrogen cooling becomes efficient. The mass

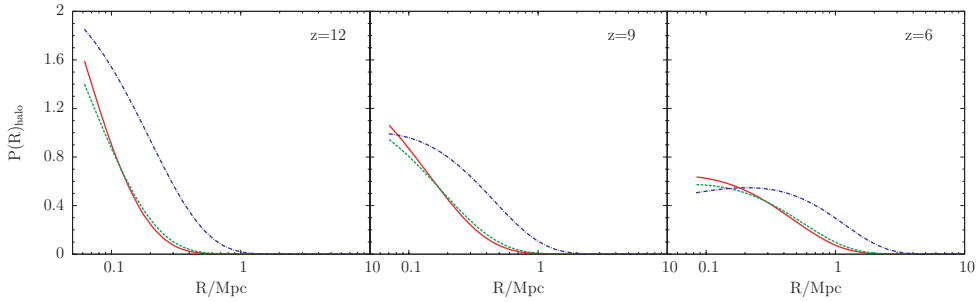

Figure 2. The halo distribution at different epochs: redshifts $z = 12, 9$ and 6 are shown in the panels, from the left-hand to right-hand side. For each cosmological model, the halo mass function is computed consistently to the PS74 formalism and written in terms of the halo radius. Different curves refer to ΛCDM model (solid line), RP model (dashed line) and SUGRA model (dot–dashed line).

associated to the ionized region is $m_{\rm H\,II} = \zeta m_{\rm gal}$, where ζ represents the ionization efficiency of the galaxy (here assumed to be constant) that depends on the star formation rate, on the escape fraction of photons and on the number of H II recombinations. Since each region is thought to be isolated, it must contain enough collapsed mass to fully ionize the inner gas. Thus, $f_{\rm coll}(\delta, m) \geqslant \zeta^{-1}$, where $f_{\rm coll}$ is the collapsed volume fraction of a region of mass $m \geqslant m_{\rm min}$ with an inner overdensity δ. In the F04 formalism, this leads to the following condition for the overdensity inside a bubble of a given mass m (in Lagrangian space):

$$\delta_m \geqslant \delta_x(m, z) \equiv \delta_c(z) - \sqrt{2}K(\zeta)[\sigma^2_{\rm min} - \sigma^2(m)]^{1/2}, \quad (6)$$

where $K(\zeta) \equiv {\rm erf}^{-1}(1 - \zeta^{-1})$, $\sigma^2(m)$ is the variance of density fluctuations smoothed on the scale m and $\sigma^2_{\rm min} \equiv \sigma^2(m_{\rm min})$. As shown in F04, δ_x represents the ionization threshold for the density fluctuations in the Lagrangian space and it is assumed to be a linear barrier with respect to $\sigma^2(m)$: $\delta_x(m, z) \sim B(m, z) = B_0(z) + B_1(z)\sigma^2(m)$. Hence, it is possible to obtain an analytic expression for the distribution of the bubbles with mass in the range $m \pm {\rm d}m/2$:

$$n(m, z) = \sqrt{\frac{2}{\pi}}\frac{\bar{\rho}}{m^2}\left|\frac{{\rm d}\ln\sigma}{{\rm d}\ln m}\right|\frac{B_0(z)}{\sigma(m)}\exp\left[-\frac{B^2(m, z)}{2\sigma^2(m)}\right], \quad (7)$$

where $\bar{\rho}$ is the mean comoving matter density of the universe. In a similar way, adopting the Lacey & Cole (1993) formalism, we can write the merger rate of the H II regions as

$$\frac{{\rm d}^2 p(m_1, m_{\rm T}, t)}{{\rm d}m_2{\rm d}t} = \sqrt{\frac{2}{\pi}}\frac{1}{t}\left|\frac{{\rm d}\ln B}{{\rm d}\ln t}\right|\left|\frac{{\rm d}\ln\sigma_{\rm T}}{{\rm d}\ln m_{\rm T}}\right|\times \left(\frac{1}{m_{\rm T}}\right)\frac{B(m_{\rm T}, z)}{\sigma_{\rm T}(1 - \sigma^2_{\rm T}/\sigma^2_1)^{3/2}}\times \exp\left[-\frac{B_0^2(z)}{2}\left(\frac{1}{\sigma^2_{\rm T}} - \frac{1}{\sigma^2_1}\right)\right], \quad (8)$$

where ${\rm d}^2 p(m_1, m_{\rm T}, t)/{\rm d}m_2{\rm d}t$ is the probability per unit time that a given halo of mass m_1 merges with a halo of mass $m_2 = m_{\rm T} - m_1$. From equation (8), it is possible to define the merger kernel

$$Q(m_1, m_2, t) \equiv \frac{1}{n(m_2, t)}\frac{{\rm d}^2 p(m_1, m_{\rm T}, t)}{{\rm d}m_2{\rm d}t}, \quad (9)$$

that represents the rate at which each region of mass m_1 merges with a region of mass m_2. Since this quantity suffers from some limitations because the asymmetry in its arguments becomes important for large masses, then the use of $Q_{\rm sym}(m_1, m_2) \equiv 1/2[Q(m_1, m_2) + Q(m_2, m_1)]$ is preferred for estimating the merger rate of the bubbles. This allows us to define the fractional volume accretion for a bubble of mass m_1 that merges with a mass m_1:

$$V(m_1)^{-1}\frac{{\rm d}V}{{\rm d}z} \equiv \frac{V(m_2)}{V(m_1)}m_2 n(m_2, z) \times Q_{\rm sym}(m_1, m_2, t)\left|\frac{{\rm d}t}{{\rm d}z}\right|. \quad (10)$$

Finally, we recall that the global ionized fraction can be calculated as $\bar{x}_i = \zeta f_{\rm coll,g}(z)$, where $f_{\rm coll,g}$ is the global collapsed volume fraction.

3.2 The recombination-limit effects

Up to now, the recombination limit has been neglected. As a bubble grows, the photons propagate more deeply into the neutral IGM, and both the clumpiness and the recombination rate of the ionized gas increase. The IGM distribution and its ionization state can be described using the analytic model of Miralda-Escudé, Haehnelt & Rees (2000) (hereafter MHR00). Analysing numerical simulations at $z < 4$, they found an analytic expression for the volume-weighted distribution of the gas density:

$$P_{\rm V}(\Delta) = A_0\Delta^{-\beta}\exp\left[-\frac{(\Delta^{-2/3} - C_0)^2}{2(2\delta_0/3)^2}\right], \quad (11)$$

where $\Delta \equiv \rho/\bar{\rho}$, δ_0 is the rms of density fluctuations smoothed on the Jeans mass at fixed z, so $\delta_0 \propto (1 + z)^{-1}$; A_0 and C_0 represent normalization constants and β can be set equal to 2.5 as predicted for isothermal spheres. The ionization state of the IGM is determined by a density threshold Δ_i such that the gas with $\Delta < \Delta_i$ is totally ionized and the gas with $\Delta > \Delta_i$ is neutral. Under this assumption, the recombination rate can be written as

$$A(\Delta_i) = A_u\int_0^{\Delta_i} P_{\rm V}(\Delta)\Delta^2{\rm d}\Delta \equiv A_u C, \quad (12)$$

where C represents the clumping factor and A_u is the recombination rate per hydrogen atom in gas at the mean density. In the F05 model, A_u is assumed consistently with the A case of the MHR00 model (see also Miralda-Escudé 2003): $A_u \propto \alpha_{\rm A}(T)$, where $\alpha_{\rm A}(10^4\,{\rm K}) = 4 \times 10^{-13}\,{\rm cm^3\,s^{-1}}$. The MHR00 model also provides a relationship between the mean free path λ_i of the photons and the ionized fraction of gas $F_{\rm V}(\Delta_i)$, namely

$$\lambda_i = \lambda_0[1 - F_{\rm V}(\Delta_i)]^{-2/3}, \quad (13)$$

where λ_0 is a normalization constant such that $\lambda_0 H(z) = 60\,{\rm km\,s^{-1}}$ at $z < 4$.

In the following, we assume that the mean free path derived in the MHR00 model could be used also in the quintessence models, since the properties of this function should reflect the gas properties at the Jeans scale, which is much smaller than the scales we are interested in. However, this approximation deserves further investigation with suitable hydrodynamical simulations.

To consider the recombination process, it is necessary to relate the recombination rate to the smoothed matter overdensity. In doing this, it must be remarked that the main effect of an inhomogeneous gas distribution is an increasing gas clumpiness and subsequently an increasing H II recombination rate. As a consequence, $A_u \propto (1 + \delta)$. When a bubble grows, the ionizing photons are able to reach its edge, and then the threshold must satisfy the condition $\lambda_i(\Delta_i) \geqslant R$ that sets Δ_i. However, at the same time, the inner high gas clumpiness causes an increase in the recombination rate and the photons can be absorbed inside the bubble before reaching the edge. For a growing region, the ionization rate then has to be larger than the recombination rate at every time:

$$\zeta\frac{{\rm d}f_{\rm coll}(\delta, R)}{{\rm d}t} > A_u C(R)(1 + \delta), \quad (14)$$

where $C(R)$ is computed as in equation (12) for $R = \lambda_i$. The recombination barrier is obtained by searching for the minimun δ in the Lagrangian space that satisfies equation (14) at each given mass.

The recombination process affects the bubbles geometry. When the ionizing photons are totally absorbed by the inner recombination, the H II region stops growing and reaches a maximum size $R_{\rm max}$ that, in a ΛCDM universe, slowly increases with decreasing redshift, as shown by F05.

In the excursion-set formalism, the recombination limit has a deep impact on the distribution of the bubbles. Assuming that the recombination barrier is a vertical line crossing δ_x at $R_{\rm max}$, the trajectories such that $\delta(R_{\rm max}) < B(R_{\rm max}, z)$ will be incorporated into H II regions

with $m < m_{\rm max}$ and the mass function reads

$$n_{\rm rec}(m, z) = \int_{-\infty}^{B(R_{\rm max})} p(\delta|R_{\rm max}) n(m, z|\delta, m_{\rm max}, z) {\rm d}\delta. \quad (15)$$

In the previous equation, $p(\delta|R_{\rm max})$ represents the probability distribution at the scale $R_{\rm max}$ for a Gaussian density field

$$p(\delta|R_{\rm max}) = \frac{1}{\sqrt{2\pi}\sigma_{\rm max}} \exp\left(-\frac{\delta^2}{2\sigma_{\rm max}^2}\right), \quad (16)$$

and $n(m, z|\delta, m_{\rm max}, z)$ is the conditional mass function for a random walk that begins at $(\delta, \sigma^2_{\rm max})$:

$$n(m, z|\delta, m_{\rm max}, z) = \sqrt{\frac{2}{\pi}} \frac{\bar{\rho}}{m^2} \left|\frac{{\rm d}\ln\sigma}{{\rm d}\ln m}\right| \times \frac{\sigma^2[B(m_{\rm max}, z) - \delta]}{(\sigma^2 - \sigma^2_{\rm max})^{3/2}} \times \exp\left\{-\frac{[B(m, z) - \delta]^2}{2(\sigma^2 - \sigma^2_{\rm max})}\right\}, \quad (17)$$

where $\sigma_{\rm max} \equiv \sigma(R_{\rm max})$. Since every trajectory lying above the ionization barrier at $R_{\rm max}$ belongs to a bubble with $R = R_{\rm max}$, the distribution of such Strömgren regions can be obtained from equation (16):

$$N_{\rm rec} = \frac{\bar{\rho}}{2m_{\rm max}} {\rm erfc}\left[\frac{B(R_{\rm max}, z)}{\sqrt{2}\sigma_{\rm max}}\right]. \quad (18)$$

After the saturation, bubbles can grow only by merging. For a single point of the IGM, reionization ends when it is incorporated in a recombination-limited region, since the ionizing background slightly increases after merging of bubbles. Thus, 'overlap' is a local phenomenon. The volume fraction of the IGM in bubbles with $R > R_{\rm max}$ is provided by the PS74 formalism using the ionization barrier and results to be

$$x_{\rm rec} = \int_{m_{\rm max}}^{+\infty} n(m, z) V(m) {\rm d}m, \quad (19)$$

where $V(m)$ is the volume of the ionized region.

3.3 The Lyman α flux transmission

The morphology of bubbles affects the absorption of the Lyman α flux emitted from high-redshift sources. Indeed, large ionized regions allow the transmission of the Lyman α forest because the extent of neutral regions in the IGM is large enough to reduce the Lyman α 'damping wing' absorption, as pointed out by Furlanetto, Hernquist & Zaldarriaga (2004b). As shown by F05, since the recombination process affects the late stages of reionization, the way how the bubbles saturate can be constrained through the Lyman flux transmission. Therefore, the observed transmitted flux from high-z galaxies can constrain the predicted evolution of H II regions.

Including the recombination limit in the F05 model allows to write the probability of having an optical depth smaller than τ_i for the ith transition, determined by the distribution of the IGM and by the morphology of the ionized bubbles, as follows:

$$P(< \tau_i) = \int_{m_{\rm H\,II\,min}}^{+\infty} n(m, z) \frac{m}{\bar{\rho}} {\rm d}m \int_0^{\Delta_{\rm max}} P_{\rm V}(\Delta) {\rm d}\Delta, \quad (20)$$

where $m_{\rm H\,II\,min}$ is the minimum mass of the H II regions and $\Delta_{\rm max}$ is the maximum density for which $\tau < \tau_i$. The analytic expression for the inner overdensity of each bubble is obtained by assuming the equation of state for the polytropic gas $T = T_0\ \Delta^\gamma$, with $T_0 = 10^4$ K and the ionization equilibrium inside each bubble. Under these assumptions, the neutral hydrogen fraction can be written as a function of the matter overdensity Δ:

$$x_{\rm H\,I} = \frac{\chi_{\rm e} \bar{n}_H \alpha(T)}{\Gamma} \Delta, \quad (21)$$

where $\chi_{\rm e}$ is the correction for the singly ionized helium and Γ is the ionizing rate per hydrogen atom. It mainly depends on the total photons' emissivity $\epsilon_{\rm T}$ and on the mean free path λ_i as

$$\Gamma \propto \lambda_i \epsilon_{\rm T} \left(\frac{\eta}{3 + \eta}\right). \quad (22)$$

At the end of reionization $\epsilon_{\rm T} \propto \zeta {\rm d}f_{\rm coll,g}/{\rm d}t$, $\eta = 3/2$ if a starburst spectrum is assumed and λ_i is set to the minimum value between the bubble radius and $R_{\rm max}$. Finally, $P_{\rm V}(\Delta)$ is thought to be independent of the bubble morphology that could be a good approximation at the end of reionization although we need high-resolution simulations to test it. Hence, the relation between the local overdensity and the IGM optical depth is

$$\Delta(\tau_i) = \left[170 \frac{\eta}{3 + \eta} \frac{\alpha_{\rm A}(10^4\,{\rm K})}{\alpha_{\rm A}(T_0)} h(z) \left(\frac{\lambda_i}{\rm Mpc}\right) \times \zeta \left|\frac{{\rm d}f_{\rm coll}}{{\rm d}z}\right| \left(\frac{\tau_i}{\tau_{{\rm GP},i}}\right)\right]^{1/(2-0.7\gamma)}, \quad (23)$$

where $\tau_{{\rm GP},i}$ is the Gunn & Peterson optical depth for the ith transition. Note that in the equation above the value of the Hubble parameter $h(z)$ is taken consistently from the different cosmological models. Finally, the probability for the inhomogeneous IGM to have a given optical depth τ is obtained by substituting $\Delta_{\rm max}$ in equation (20).

A warning has to be kept in mind regarding the application of our model to derive the Lyman fluxes. Some of the simplifying assumptions present in the description of the recombination process, like the abrupt change in the IGM ionization state as a function of its density (see e.g. discussion in Miralda-Escudé et al. 2000). We expect, however, that a more realistic treatment would change our predictions in the same way for the different cosmological models. For this reason, we prefer to present our results in terms of ratios between the fluxes derived for the quintessence models and those predicted for the ΛCDM model.

4 RESULTS AND DISCUSSION

In this section, we present the main results of the application of the previous model to cosmological scenarios including a dynamic quintessence (see Section 2). Note that F04 and F05 apply their model to the 'concordance' ΛCDM model only.

First of all, we compute the minimum collapsed mass at each cosmological epoch from the mass–temperature relation proposed by Barkana & Loeb (2001):

$$T_{\rm vir} = 1.98 \times 10^4 \left(\frac{\mu}{0.6}\right) \left(\frac{M}{10^8 h^{-1} {\rm M}_\odot}\right)^{2/3} \times \left[\frac{\Omega_{\rm m}}{\Omega_{\rm m}^z} \frac{\Delta_c}{18\pi^2}\right]^{1/3} \left(\frac{1 + z}{10}\right) {\rm K}, \quad (24)$$

where $T_{\rm vir}$ is the virial temperature of a halo having mass M and μ is the mean molecular weight of its inner gas. In order to take into account the fact that the IGM inside a H II region is not totally ionized because of the ionization equilibrium assumption, here we prefer to set μ to the mean of the values discussed in Barkana & Loeb (2001). Anyway, we checked that fixing the molecular weight to the

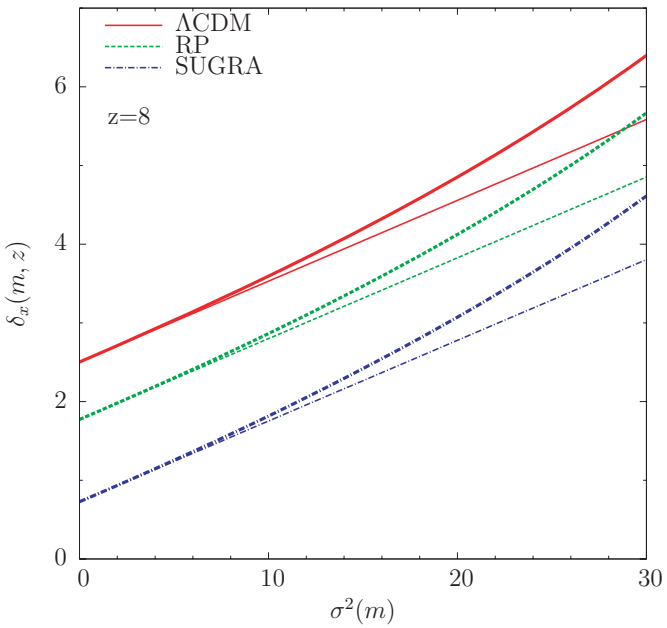

Figure 3. The ionization barrier is here shown at $z = 8$, assuming an ionization efficiency of $\zeta = 6$. For each cosmological model, the thick line represents δ_x as defined in equation (6), while the thin line is its linear approximation. The curves refer to the ΛCDM model (solid line), RP model (dashed line) and SUGRA model (dot–dashed line).

value corresponding to a fully ionized IGM ($\mu = 0.6$) does not significantly affect the model predictions on the observables discussed at the end of this section. For example, using $\mu = 0.6$ changes the Lyman α flux transmission by ∼1 per cent only, irrespective of the considered cosmological model.

The values for Δ_c and for the redshift evolution of $\Omega_m(z)$ are computed consistently for the different cosmologies. The presence of a dynamic quintessence component affects the hierarchic evolution of the ionized regions. Indeed, the earlier growth of matter perturbations causes, at a fixed epoch, the formation of larger ionized regions in the quintessence cosmology. Another important consequence is that, even if the assumption of a linear ionization barrier is still correct, this is lower than in the ΛCDM universe. This is evident in Fig. 3, where we show the behaviour of the ionization barrier in the three different cosmological models, computed at $z = 8$, assuming $\zeta = 6$.

This implies a higher probability that matter fluctuations go beyond the ionization threshold. Consequently, the density of bubbles increases, resulting in a different morphology of H II regions in the three cosmologies considered, as shown in Fig. 4. The earlier growth of the matter fluctuations in the quintessence models causes a faster evolution of the mass function with respect to the ΛCDM universe and a remarkable increase in the density of the largest regions. As a consequence, at the same cosmological epoch, we obtain a higher ionized fraction $\bar{x}_i$ in the quintessence cases. As an illustrative example, we observe that at $z = 8.8$, reionization is at its initial phases in the 'standard' universe ($\bar{x}_i = 0.35$) while for the SUGRA cosmology this epoch corresponds to its late stages, $\bar{x}_i = 0.65$. This is almost a factor of ∼2 larger than in the 'standard' case. Similarly, at $z = 8$ reionization is at the final stage in the SUGRA universe, $\bar{x}_i = 0.82$, while $\bar{x}_i = 0.47$ for the 'concordance' model. We recall that the model we adopt, being based on the extended PS74 formalism, can account only in a very approximate way, most often in the linear limit, for the source clustering, which is expected to have important effects on the morphology of the H II regions. Since the clustering amplitude depends on the source abundances which are different in the models considered here, our results could be affected by this bias. Work is in progress to properly address this problem by improving our modelling with suitable numerical simulations.

In Fig. 5, we show the different characteristic sizes, $R_{\rm char}$, of the ionized regions, as obtained by fixing ζ such that reionization ends at $z = 6$ (note that ζ is not the same for the three models). Neglecting the recombination limit, the effects of the quintessence are obvious at the early stages of reionization, since $R_{\rm char}$ (representing the radius for which the bubbles distribution is maximum) is larger in the standard universe than in RP and SUGRA models. For example, at $x_i \simeq 0.2$ $R_{\rm char} = 0.4$ and 0.6 Mpc for ΛCDM and SUGRA, respectively. But the difference becomes increasingly smaller as reionization proceeds. This is caused by the different saturation regime of the IGM in the quintessence cosmologies. Ionized regions are smaller in the RP and SUGRA models at the beginning of reionization and their sizes evolve faster than in the ΛCDM universe due to the presence of large neutral voids around them, reaching the characteristic radius of the standard model in the final stages of reionization.

Since the H II regions grow only by merging after the recombination limit, it is interesting to investigate how the dynamic dark energy component affects the bubbles' merger rates. As an example, Fig. 6 shows the merger probability of a region with mass $M = 10^{14}$ $M_\odot$ at $z = 13$ for the ΛCDM, RP and SUGRA universes. Similarly to the ΛCDM case, also for the quintessence cosmologies the evolution

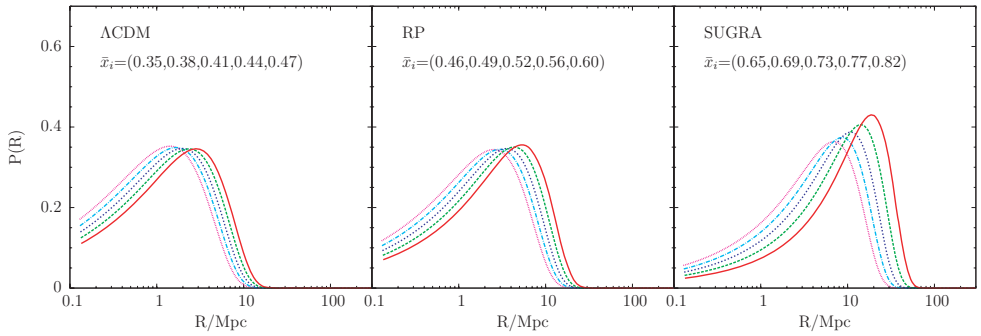

Figure 4. The morphology of the H II regions. The probability distribution of the bubble sizes is computed here neglecting recombination. In each panel (corresponding to different cosmological models), the curves refer to different epochs: $z = 8.8$ (dotted line), 8.6 (dot–dashed line), 8.4 (short-dashed line), 8.2 (long-dashed line) and 8 (solid line). The corresponding values for the ionized volume fraction $\bar{x}_i$, computed assuming a ionization efficiency $\zeta = 6$, are also reported.

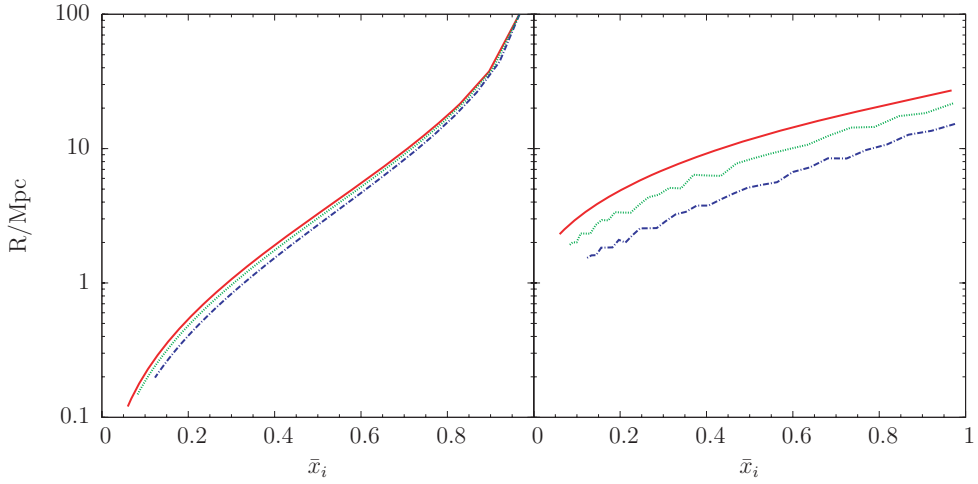

Figure 5. The bubble morphology. The evolution of the bubble radius as a function of $\bar{x}_i$ is shown here neglecting recombination (left-hand panel) and in the recombination limit (right-hand panel). The solid, dotted and dot–dashed lines are for ΛCDM, RP and SUGRA models, respectively. A complete reionization at $z = 6$ is assumed here.

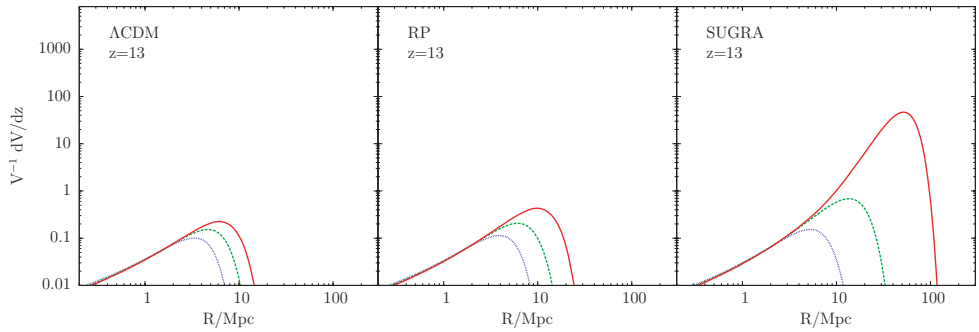

Figure 6. The hierarchic growth of bubbles. In each panel (corresponding to different cosmological models), we show the fractional volume accretion rate of an H II region having mass $M_1 = 10^{14}\,\mathrm{M}_\odot$ that merges with a mass corresponding to a given radius R. The results, computed at $z = 13$, are obtained assuming different ionization efficiencies: $\zeta = 10$ (dotted line), $\zeta = 20$ (dashed line) and $\zeta = 30$ (solid line).

of the bubbles is dominated by merging events between large systems, in particular in the late stages of the reionization process. The main difference is given by the size of the involved regions. For the RP and SUGRA models, the merger probability is higher with bubbles that are even one order of magnitude larger than in the standard universe.

We can now investigate how the recombination limit due to the IGM clumpiness affects the geometry and the evolution of the ionized regions in the quintessence universes. As already said, in doing this, we assume that the results of the MHR00 simulations obtained for a standard cosmology are still valid for a dynamic dark energy dominated universe, since we do not expect large differences for the IGM volume-weighted density distribution. As discussed above, the dark energy component causes the matter fluctuations to grow earlier. Hence, since the recombination rate depends on the inner overdensity of the bubbles, recombination is strong already at smaller scales in the quintessence universe, compared to the ΛCDM case. Thus, the H II regions reach the equilibrium on scales smaller than in the standard model. This is clear in Fig. 7, where we present three different stages of reionization. While the ionization threshold does not significantly change between ΛCDM and SUGRA models, the recombination barrier $\delta_{\rm rec}$ extends to smaller scales in the quintessence universes. This effect is more prominent at the late stages of reionization process, since the bubbles reach the equilibrium on scale of the order of 20–30 Mpc in the ΛCDM universe instead of the ∼10 Mpc predicted for SUGRA. In dynamic dark energy universes, the 'earlier' (in term of comoving scales) recombination barrier involves a smaller value for $R_{\rm max}$, computed as the cross-point of δ_x and $\delta_{\rm rec}$. The same trend was already evident in Fig. 5, where the assumed values for ζ were such that $\bar{x}_i(z = 6) = 1$. A peculiarity with respect to the standard model is the discontinuous recombination barrier found for the SUGRA cosmology that crosses the ionization threshold more than once. To avoid further complications to the model, we choose to set $R_{\rm max}$ to the mean value of those achieved at the cross-points (which are in any case very close to each other).

Fig. 8 shows an important effect on the bubble distribution of the fact that the maximum radius is smaller, illustrated at $z = 8$ for different stages of reionization. As a result, the H II regions with $M < M_{\rm max}$ tend to pile up on $\lesssim$10 Mpc scales in the SUGRA universe, in particular at the end of reionization. Furthermore, the drop in the ionization threshold causes an increase in the volume fraction contained in the recombination-limited regions.

As mentioned before, for a random point in the IGM, the reionization process can be considered complete when the point joins a sphere with $M = M_{\rm max}$. Since $R_{\rm max}$ is smaller in the quintessence cosmologies, the density of the points belonging to a region with $M > M_{\rm max}$ increases and the volume fraction inside bubbles larger

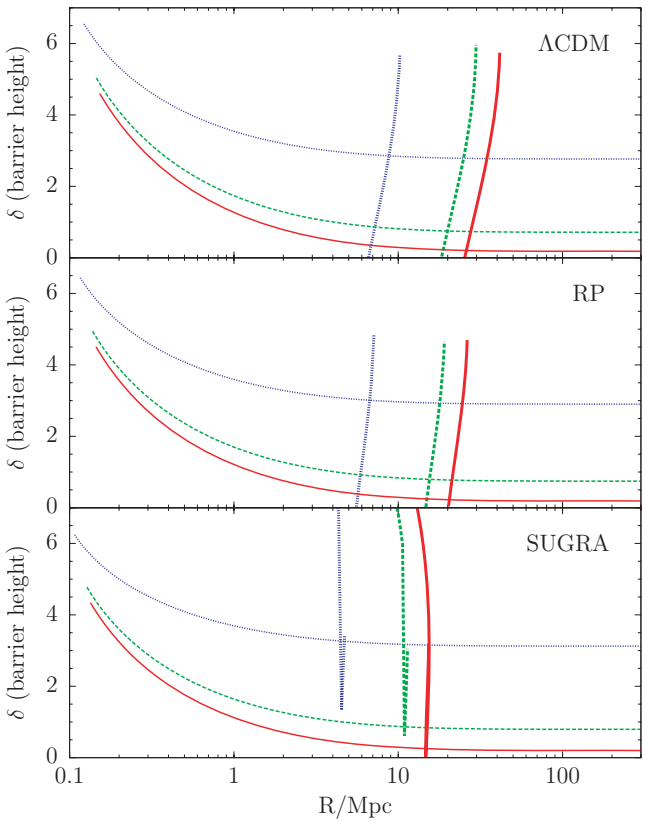

Figure 7. The recombination limit. In each panel (corresponding to different cosmological models), we show the ionization barrier, computed as in F04 (thin curves), and the recombination barrier, computed as in F05 (thick curves). The results are shown at three different stages of reionization: $\bar{x}_i = 0.49$ (dotted lines), $\bar{x}_i = 0.82$ (dashed lines) and $\bar{x}_i = 0.95$ (solid lines) at $z = 6$.

than $M_{\rm max}$ becomes larger. As shown in Fig. 9, $x_{\rm rec}$ increases moving from the ΛCDM to the SUGRA models as reionization proceeds involving different 'epochs of overlapping'. In this case, $x_{\rm rec} \sim 0.5$ is reached earlier in the quintessence models than in the standard universe. This effect is analogous to that discussed by F05 for a small mean free path of the ionizing photons.

As illustrated before, the bubble morphology and the IGM ionization state affect the IGM optical depth τ and consequently the transmission of the Lyman α flux. To investigate how the IGM optical depth distribution depends on $R_{\rm max}$ in the quintessence models, we compute the probability distribution $p(\tau)$ of the IGM optical depth for the Lyman α, *Lyman* β and Lyman γ transmission following equation (20). In Fig. 10, we compare $p(\tau)$ for the RP and SUGRA scenarios to that obtained considering the ΛCDM model, $p(\tau)_{\Lambda\rm CDM}$, for different values of $R_{\rm max}$. The transmission is lower for small values of τ. We find that the trends with $R_{\rm max}$ for the Lyman β (central panels) and Lyman γ (lower panels) are analogous to that for the Lyman α one (upper panels).

5 CONCLUSIONS

The purpose of this work is to give a picture of the reionization epoch in the universes dominated by a dynamic dark energy component at late epochs, tracing the H II region evolution using an analytic approach based on the hierarchic growth of matter fluctuations. In doing this, we consider two cosmological models in which the dark energy density varies with time driven by the RP and Brax & Martin (2000) potentials. We then used the analytic approach proposed by F05 to outline the main differences between the evolution of bubbles in the quintessence models and in the standard ΛCDM cosmology. Our results can be summarized as follows.

(1) The growth of density fluctuations occurs earlier and the ionization barrier δ_x is lower in the RP and SUGRA universes compared to the ΛCDM one. This causes a strong increase in the high-density regions with respect to the ΛCDM case at the same epoch.

(2) Neglecting the recombination limit, the characteristic size of the H II regions is smaller in the RP and SUGRA cases at the early stage of reionization, but the difference is weakened as reionization proceeds.

(3) In the recombination limit, the early growth of the matter fluctuations causes the increase in the IGM clumpiness and the inner recombination of the bubbles becomes more efficient. As a consequence, the H II regions reach the ionization equilibrium on slightly smaller scales and the bubble abundance tends to increase. The IGM volume fraction contained in bubbles larger than $R_{\rm max}$ increases, producing an earlier 'epoch of overlap' in the quintessence universe compared to ΛCDM.

(4) The main effect on the high-z QSO radiation transmission due to the different evolution of the H II regions is the lower Lyman flux absorption at small optical depths in RP and SUGRA cosmologies compared to the ΛCDM model.

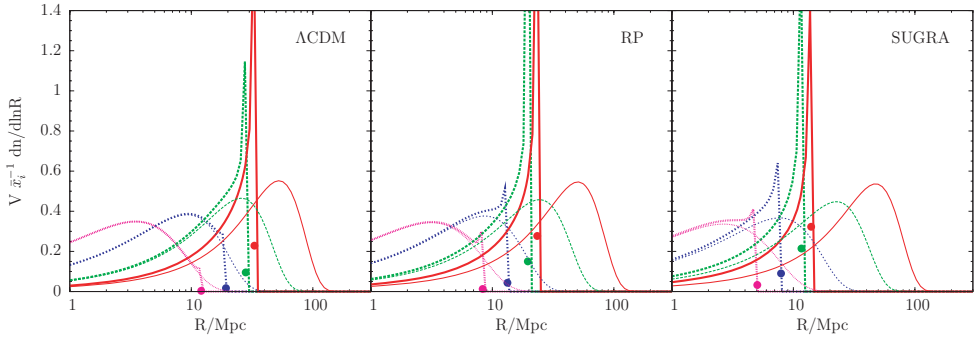

Figure 8. The bubble size distribution considering the recombination process. The mass distributions show that in the recombination limit (thick curves) bubbles pile up at $R = R_{\rm max}$, while neglecting recombination (thin curves) they can reach sizes larger than $R_{\rm max}$. In each panel (corresponding to different cosmological models), the different curves refer to the H II region distribution at different stages of reionization: $\bar{x}_i = 0.51$ (dotted line), $\bar{x}_i = 0.68$ (short-dashed line), $\bar{x}_i = 0.84$ (long-dashed line), $\bar{x}_i = 0.92$ (solid line) assumed for $z = 8$. The filled points represent the volume fraction in bubbles with $R = R_{\rm max}$ in the recombination limit.

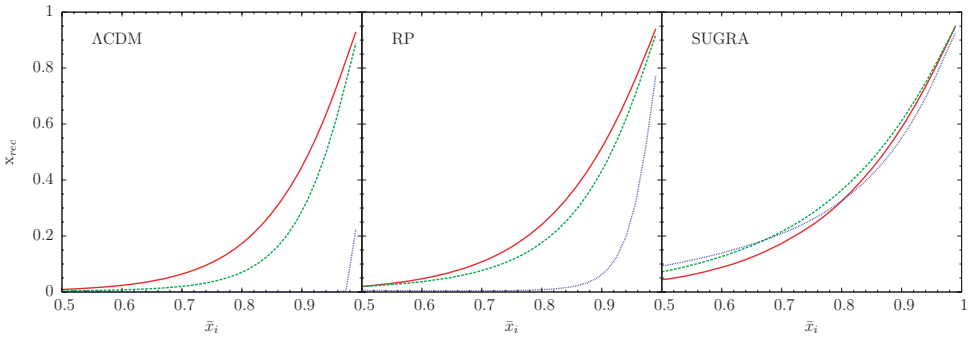

Figure 9. The ionized volume fraction. In each panel (corresponding to different cosmological models), the curves refer to the volume fraction contained in recombination-limited bubbles during the overlap phase at different redshifts: $z = 6$ (solid line), $z = 9$ (dashed line) and $z = 12$ (dotted line). The results are computed assuming the MHR00 model with $\lambda_0 = 60\,\mathrm{km\,s^{-1}}$.

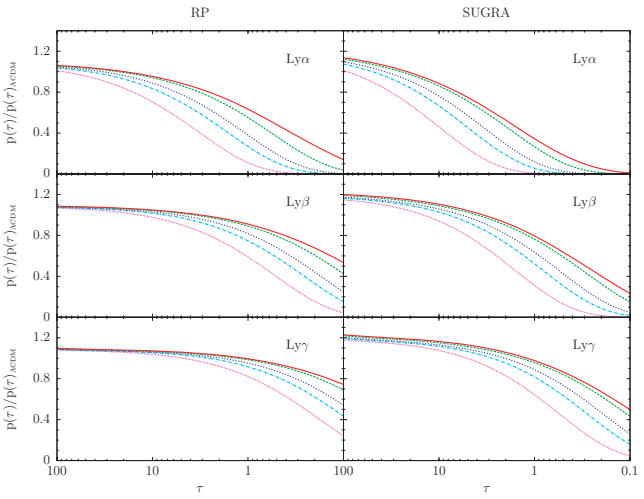

Figure 10. The Lyman transitions. The probability distribution of the IGM optical depth $p(\tau)$ for the quintessence models is compared to that in the 'standard' universe ($p(\tau)_{\Lambda\mathrm{CDM}}$). Results for the RP and SUGRA models are shown in the panels in the left-hand and right-hand columns, respectively, and refer to Lyman α, Lyman β and Lyman γ, in the different panels, from top to bottom. The curves are computed in the case of complete reionization ($\bar{x}_i = 0.95$) at $z = 6$ for different values of R_{max}: 10 Mpc (dotted line), 20 Mpc (dot–dashed line), 30 Mpc (short-dashed line), 60 Mpc (long-dashed line) and 600 Mpc (solid line).

ACKNOWLEDGMENTS

We acknowledge financial contribution from contracts ASI-INAF I/023/05/0, ASI-INAF I/088/06/0 and INFN PD51. We thank Steven Furlanetto, Peng Oh, James Bolton, Enzo Branchini and Micol Bolzonella for useful discussions. We thank the anonymous referee for her/his constructive comments.

REFERENCES

Barkana R., Loeb A., 2001, Phys. Rep., 349, 125
Barkana R., Loeb A., 2004, ApJ, 609, 474
Becker G. D., Rauch M., Sargent W. L. W., 2007, ApJ, 662, 72
Becker R. H. et al., 2001, AJ, 122, 2850
Bolton J. S., Haehnelt M. G., 2007, MNRAS, 381, L35
Brax P., Martin J., 2000, Phys. Rev. D, 61, 103502
Choudhury T. R., Ferrara A., 2006, in Fabbri R., ed., Cosmic Polarization. Research SignPost, p. 205
Ciardi B., Ferrara A., 2005, Space Sci. Rev., 116, 625
Ciardi B., Ferrara A., White S. D. M., 2003, MNRAS, 344, L7
Ciardi B., Stoehr F., White S. D. M., 2003, MNRAS, 343, 1101
Dolag K., Bartelmann M., Perrotta F., Baccigalupi C., Moscardini L., Meneghetti M., Tormen G., 2004, A&A, 416, 853
Fan X. et al., 2001, AJ, 122, 2833
Fan X. et al., 2006, AJ, 132, 117
Furlanetto S. R., Oh S. P., 2005, MNRAS, 363, 1031 (F05)
Furlanetto S. R., Zaldarriaga M., Hernquist L., 2004a, ApJ, 613, 1 (F04)
Furlanetto S. R., Hernquist L., Zaldarriaga M., 2004b, MNRAS, 354, 695
Gnedin N. Y., 2000, ApJ, 535, 530
Haiman Z., Holder G. P., 2003, ApJ, 595, 1
Hui L., Haiman Z., 2003, ApJ, 596, 9
Iliev I. T., Mellema G., Pen U.-L., Merz H., Shapiro P. R., Alvarez M. A., 2006, MNRAS, 369, 1625
Iliev I. T., Mellema G., Shapiro P. R., Pen U.-L., 2007, MNRAS, 376, 534
Kashikawa N. et al., 2006, ApJ, 648, 7
Lacey C., Cole S., 1993, MNRAS, 262, 627
Liddle A. R., Mukherjee P., Parkinson D., Wang Y., 2006, Phys. Rev. D, 74, 123506
Lukic Z., Heitmann K., Habib S., Bashinsky S., Ricker P. M., 2007, ApJ, 671, 1160
Madau P., Rees M. J., Volonteri M., Haardt F., Oh S. P., 2004, ApJ, 604, 484
Maio U., Dolag K., Meneghetti M., Moscardini L., Yoshida N., Baccigalupi C., Bartelmann M., Perrotta F., 2006, MNRAS, 373, 869
Malhotra S., Rhoads J. E., 2004, ApJ, 617, L5
Meneghetti M., Bartelmann M., Dolag K., Moscardini L., Perrotta F., Baccigalupi C., Tormen G., 2005, A&A, 442, 413
Miralda-Escudé J., 2003, ApJ, 597, 66
Miralda-Escudé J., Haehnelt M., Rees M. J., 2000, ApJ, 530, 1 (MHR00)
Peebles P. J., Ratra B., 2003, Rev. Mod. Phys., 75, 559 (RP)
Press W. H., Schechter P., 1974, ApJ, 187, 425
Reed D. S., Bower R., Frenk C. S., Jenkins A., Theuns T., 2007, MNRAS, 374, 2
Riess A. G. et al., 2007, ApJ, 659, 98
Sokasian A., Abel T., Hernquist L., Springel V., 2003, MNRAS, 344, 607
Sokasian A., Yoshida N., Abel T., Hernquist L., Springel V., 2004, MNRAS, 350, 47
Spergel D. N. et al., 2003, ApJS, 148, 175
Spergel D. N. et al., 2007, ApJS, 170, 377
White R. L., Becker R. H., Fan X., Strauss M. A., 2003, AJ, 126, 1
Wyithe J. S. B., Cen R., 2007, ApJ, 659, 890
Wyithe J. S. B., Loeb A., 2003, ApJ, 586, 693

This paper has been typeset from a TEX/LATEX file prepared by the author.